Elastic scattering and breakup of ^{11}Be on deuterons at 26.9A MeV

J. Chen,[1] J. L. Lou,[1,*] Y. L. Ye,[1] J. Rangel,[2] A. M. Moro,[3] D. Y. Pang,[4] Z. H. Li,[1] Y. C. Ge,[1] Q. T. Li,[1] J. Li,[1] W. Jiang,[1] Y. L. Sun,[1] H. L. Zang,[1] Y. Zhang,[1] N. Aoi,[5] E. Ideguchi,[5] H. J. Ong,[5] J. Lee,[6] J. Wu,[6] H. N. Liu,[6] C. Wen,[6] Y. Ayyad,[5] K. Hatanaka,[5] T. D. Tran,[5] T. Yamamoto,[5] M. Tanaka,[5] T. Suzuki,[5] and T. T. Nguyen[5]

[1]*School of Physics and State Key Laboratory of Nuclear Physics and Technology, Peking University, Beijing 100871, China*

[2]*Instituto de Física, Universidade Federal Fluminense, Avenida Litoranea s/n, Gragoatá, 24210-340, Niterói, Rio de Janeiro, Brazil*

[3]*Departamento de FAMN, Universidad de Sevilla, Apartado 1065, 41080 Sevilla, Spain*

[4]*School of Physics and Nuclear Energy Engineering, Beijing Key Laboratory of Advanced Nuclear Materials and Physics, Beihang University, Beijing 100191, China*

[5]*Research Centre for Nuclear Physics, Osaka University, Osaka, Japan*

[6]*RIKEN (Institute of Physical and Chemical Research), 2-1 Hirosawa, Wako, Saitama 351-0198, Japan*

(Received 31 August 2016; published 30 December 2016)

The elastic scattering and breakup reactions of the halo nucleus ^{11}Be on deuterons at an incident energy of 26.9A MeV are reported for the first time. Special attention has been paid to the determination and subtraction of the proton contaminations in the deuterated polyethylene $(CD_2)_n$ target (where D_2 denotes $^2H_2$). The cross sections for elastic scattering are analyzed with the systematic optical potentials of Daehnick *et al.* and DA1p, as well as with single-folding potentials, derived from the Jeukenne-Lejeune-Mahaux effective nucleon-nucleon interaction. An extended version of the continuum-discretized coupled-channels (XCDCC) formalism, including dynamic core excitation (DCX) effects, is applied to analyze the elastic scattering and breakup data. Comparisons of the full XCDCC calculation with that omitting DCX effects indicate that the core excitation plays a remarkable role in reproducing breakup reactions of ^{11}Be $+d$.

DOI: 10.1103/PhysRevC.94.064620

I. INTRODUCTION

The investigation of exotic nuclei has continuously developed since the early 1980s thanks to the availability of various tools for radioactive beam production, including in-flight fragmentation, which provide ever increasing accessibility of the nuclear landscape far from the β-stability line [1–3]. ^{11}Be was extensively studied as a neutron-halo nucleus. Its small one-neutron separation energy of 504 keV together with the dominant s-wave configuration of the valence neutron lead to a very extended neutron-density distribution [4–6]. The parity inversion of its ground state $(1/2^+)$ was predicted by Talmi and Unna [7] and confirmed by the experimental measurement of Alburger *et al.* [8]. Numerous measurements and structure calculations suggest that the ground state of ^{11}Be contains, in addition to the dominant $^{10}\mathrm{Be}(0^+) + n(s_{1/2})$ configuration, a significant admixture ($\sim$20%) of core excited components, with the valence neutron preferably occupying the $d_{5/2}$ orbit [9–11].

The sizable core excitation components in the ^{11}Be ground state play an important role in featuring the ^{11}Be structure. Furthermore, when considering the collision of ^{11}Be on a target, the coupling between the collective excitations and the core excitations would affect the reaction dynamics. Both effects (structure and dynamics) have been implemented in an extended version of the continuum-discretized coupled-channels (XCDCC) formalism proposed by Summers *et al.* [12], and in a no-recoil extended distorted wave Born approximation (XDWBA) model [13]. Core excitation was shown to have a significant effect on the breakup cross sections in calculations using the XCDCC model for the breakup of ^{11}Be on a proton target at incident energies of 63.7 [13–15] and 26.9A MeV [16]. These two measurements confirmed the core excitation effects at various incident energies. Furthermore, core excitation was demonstrated to be important on various tightly bound targets, like ^{1}H [13–15], ^{12}C [11], ^{64}Zn [17,18], and ^{208}Pb [11]. It is interesting to examine the core excitation effect on the weakly bound targets, such as a deuteron target.

Historically, the deuteron, as a typical weakly bound nucleus, is of great importance in nuclear reaction study. Most direct nuclear reactions, such as stripping, transfer, and pickup, were first studied with deuteron beams due to their easy access by accelerators. Deuteron-induced reactions have been one of the most powerful spectroscopic tools to extract structure information of stable nuclei. These studies can be extended to the case of unstable nuclei, using experiments in inverse kinematics. For unstable projectiles close to the drip lines, the description of these reactions is, however, challenging because one has to treat coupling arising from both the projectile and target breakup. The measurement of these kinds of data, along with the modification of related reaction formalisms to describe them, is therefore a topic of timely interest to reliably extend the spectroscopic studies with deuterons to regions far from the stability line.

In this work, we present the data of elastic scattering and breakup of ^{11}Be, for the first time, on a deuteron target at 26.9A MeV. The beam energy was chosen considering the validity of both breakup and transfer reaction mechanisms, the availability of the beam, the effective detection of recoil light charged particles at large angles, and the complement to the previous breakup reaction work at higher energy [19]

*jllou@pku.edu.cn

and transfer reaction experiments at lower energies [20,21]. The paper is organized as follows. In Sec. II we present the details of the experiment, and the data analysis. Special attention is paid to the determination and subtraction of the proton contaminations in the $(CD_2)_n$ target (where D_2 denotes $^2H_2$). In Sec. III we show an optical model analysis of the elastic scattering data in terms of phenomenological optical potentials. In Sec. IV the angular distributions of elastic scattering and breakup are compared with the XCDCC calculations, and the importance of the core excitation effect is also discussed. Finally, in Sec. V we summarize the main results of this work.

II. EXPERIMENTAL RESULTS

The experiment was performed on the EN-course beam line at the Research Center for Nuclear Physics (RCNP), Osaka University, Japan [22]. The primary beam ^{13}C at 60A MeV impinged on a thick ^9Be target to produce a secondary beam of ^{11}Be, which was separated and purified by the electromagnetic separator. The beam intensity and purity for ^{11}Be was approximately 1×10^4 particles per second and 95%, respectively. The momentum spread was limited, by a slit at the dispersion plane, down to $\Delta P/P = 1\%$ to reduce the energy spread of the beam. The beam spot size on the physical target is less than $\phi 20$ mm.

The experimental setup can be found in Ref. [16], and only detectors relevant to the elastic scattering and breakup of $^{11}Be + d$ are described here. Telescopes TELE0 and TELE1 were employed to detect the projectlike isotopes and the recoil light particles, respectively. TELE0, comprising a double-sided silicon strip detector (DSSD) with a thickness of 1000 μm and two large surface silicon detectors (SSDs) 1500 μm thick, was installed at around 0° relative to the beam direction. TELE1 is composed of a 300-μm DSSD, a 1500-μm SSD, and a layer of four CsI(Tl) crystals read out by photodiodes. The active area and strip width of each DSSD is 62.5×62.5 mm^2 and 2 mm, respectively. The distance between the center of the target and TELE0 (TELE1) is 200 (170) mm. A $(CD_2)_n$ target with a thickness of 4 mg/cm^2 was mounted as the physical target, together with a carbon film (12 mg/cm^2) and also a $(CH_2)_n$ foil (4 mg/cm^2) used for background measurements. The $(CD_2)_n$ target thickness is optimized in order to have enough recoil deuteron yield while retaining good resolution for excitation energies in ^{11}Be deduced from the recoil deuterons. Targets were tilted 15° to restrict the energy loss of the recoil light particles in the target. For deuterons elastically scattered to 81.5°, corresponding to the minimum detection angle in the center-of-mass system (16.5°) for ^{11}Be, the recoil deuteron energy is 3.3 MeV while its energy loss in the target is about 1.19 MeV, assuming the reaction point at the middle of the tilted target, which is good enough to meet the detection and resolution requirements. In coincidence with the recoil light particles, the residual fragments were identified with $\Delta E - E$ method. ^{10}Be is well separated from ^{11}Be as shown in the particle identification (PID) spectrum in Fig. 1. The differential cross sections of the $^{11}Be + d$ elastic scattering and breakup can be extracted from the recoil deuterons in coincidence with ^{11}Be and ^{10}Be, respectively.

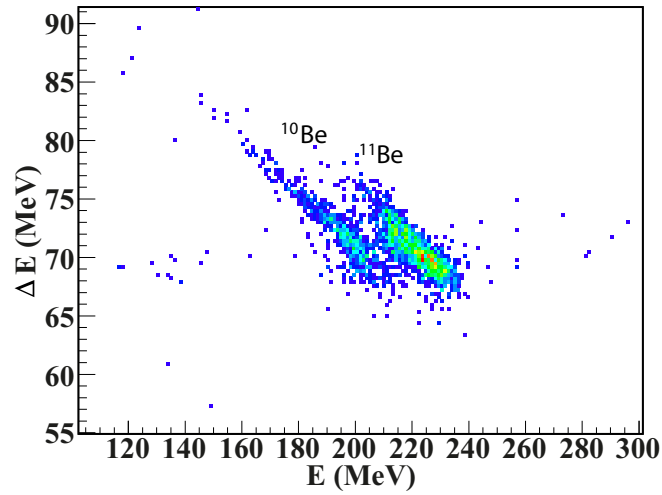

FIG. 1. The PID using data taken by TELE0 in coincidence with light particles measured by TELE1.

Figures 2(a) and 2(b) illustrate energies versus angles of the recoil light particles (proton and deuteron) measured by TELE0 in coincidence with ^{11}Be and ^{10}Be detected by TELE1, respectively. The energy losses of deuterons in the target were corrected for the deduced excitation energy spectra in Fig. 2, assuming a reaction point at the middle of the target. A cut of laboratory angles smaller than 80° was applied due to the energy detection threshold for the recoil light particles. Most events lie along the kinematic curves for the $^{11}Be + d$ elastic (solid curve) and inelastic scattering (dashed and dotted curves), but a small portion of events distribute around the kinematic lines of $^{11}Be + p$ (dot-dot-dashed curve). The reason is that the deuterated compounds are usually contaminated by some hydrogen component, whose contributions should be subtracted from the experimental data of ^{11}Be scattered from the $(CD_2)_n$ target. In addition, these events could also

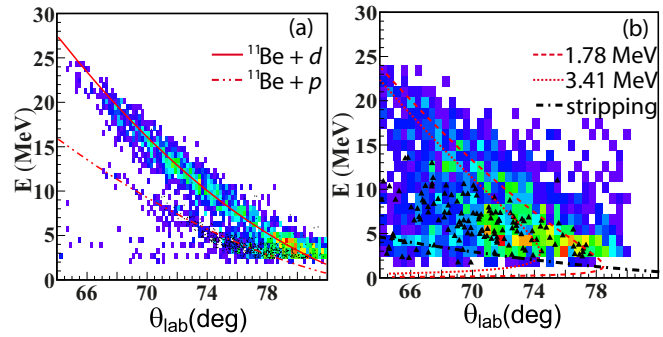

FIG. 2. Plot of energy vs angle for the recoil light particles in coincidence with (a) ^{11}Be and (b) ^{10}Be for $(CD_2)_n$ (color palettes) and $(CH_2)_n$ (black dots and triangles) targets. The calculated kinematic loci for the elastic scattering of $^{11}Be + d$ and $^{11}Be + p$ are shown as solid and dot-dot-dashed curves in (a), while that for the $^{11}Be + d$ inelastic scattering to the 1.78- and 3.41-MeV resonances of ^{11}Be are represented as dashed and dotted curves in (b), respectively. The dot-dashed line stands for the kinematic curve for the n-d elastic scattering.

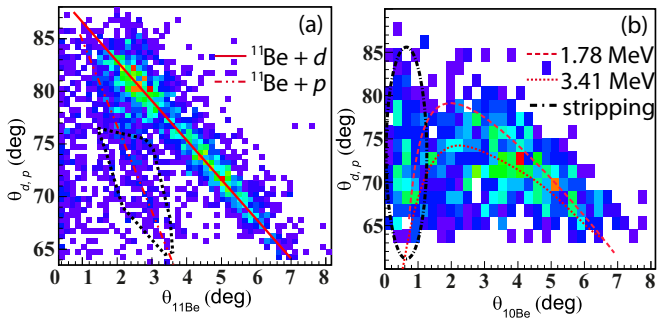

FIG. 3. Angular correlation spectra for the recoil light particles and the elastic scattered (a) ^{11}Be, and (b) ^{10}Be from the breakup reaction, respectively, on the impure $(CD_2)_n$ target. The definitions of kinematic curves are the same as those in Fig. 2. The area marked by dotted curves in (a) shows the cut applied for the calculation of proton contaminations. The black dot-dashed circle in (b) represents the area for the $1n$ stripping reaction from ^{11}Be by the $(CD_2)_n$ target.

be observed on the angular correlation spectra for the recoil light particles and ^{11}Be [see dot-dot-dashed curve in Fig. 3(a)]. Considering that the Rutherford cross section for ^{11}Be $+p$ is about four times larger than that for ^{11}Be $+d$ at the same laboratory angles, we could infer that the ^{11}Be $+p$ elastic scattering cross section is much larger than that of ^{11}Be $+d$. As a result, even if the hydrogen contamination is small in the $(CD_2)_n$ target, its influence should not be ignored, especially in the small center-of-mass angles of ^{11}Be or large laboratory angles of deuterons [see Fig. 3(a)], where the scattered protons are mixed with deuterons. This effect can be removed by subtracting the $(CH_2)_n$ target experimental data from the $(CD_2)_n$ data as long as we know the fraction of proton contaminant in the $(CD_2)_n$ target.

Based on the fact that ^{11}Be $+p$ elastic scattering differential cross sections are the same for protons in $(CH_2)_n$ and impure $(CD_2)_n$ targets, and the detectors (solid angles) are the same during $(CH_2)_n$ and $(CD_2)_n$ target experiments, the following equation can be established:

$$\frac{\rho_{\text{H-CD}_2}}{\rho_{\text{H-CH}_2}} = \frac{N_{\text{SH-CD}_2}}{N_{\text{SH-CH}_2}} \frac{N_{\text{in-CH}_2}}{N_{\text{in-CD}_2}}, \tag{1}$$

where $\rho_{\text{H-CH}_2}$ ($\rho_{\text{H-CD}_2}$), $N_{\text{SH-CH}_2}$ ($N_{\text{SH-CD}_2}$), and $N_{\text{in-CH}_2}$ ($N_{\text{in-CD}_2}$) stand for the proton areal density (mg/cm^2), the elastically scattered proton number, and the incoming ^{11}Be beam particle number for the $(CH_2)_n$ [$(CD_2)_n$] target, respectively. Since the thickness of the $(CH_2)_n$ target is known (4.0 mg/cm^2), the density of proton contaminations in the $(CD_2)_n$ target can be determined by the ratio of the scattered protons in $(CH_2)_n$ and $(CD_2)_n$ targets with the normalized ^{11}Be particle number. In order to calculate $\rho_{\text{H-CD}_2}$ we applied a cut (black dotted area) on Fig. 3(a) where the protons are clearly separated from the deuterons and most events follow the kinematic curve for the ^{11}Be $+p$ angular correlations (dot-dot-dashed curve). With this cut, the ^{11}Be excitation energy spectra are deduced from energies and angles of the protons measured from the $(CH_2)_n$ and the contaminated $(CD_2)_n$ targets. Finally, for the contaminated $(CD_2)_n$ target with a total thickness of 4.0 mg/cm^2 used in this experiment, the ratio of proton and deuteron number is determined to be $9.5 \pm 0.6\%$. The error 0.6% is obtained from the statistics of the scattered light particles number, and the incoming beam particles number. The systematic error is estimated to be 1.2% mainly resulting from the different cuts in Fig. 3(a) and the uncertainties in target thickness.

In Sec. IV, the measured breakup data are compared with XCDCC calculations. Because this method provides only the elastic breakup cross sections, the contributions from other reaction processes should be removed from the breakup experimental results. Similarly to Ref. [16], the coincident measurement of the recoil deuterons and ^{10}Be can help us exclude the contributions of $1n$ stripping from ^{11}Be using the kinematic conditions. Some details can be seen in Figs. 2(b) and 3(b). First, the neutron stripped from the ^{11}Be projectile by the deuteron target would approximately follow the kinematics of the n-d elastic scattering, as shown by the black dot-dashed curve in Fig. 2(b). Second, after the $1n$ stripping reaction, the residual ^{10}Be fragments would be emitted around 0° relative to the beam direction. At laboratory angles smaller than 1.2°, a small fraction of events are clearly separated from the angular correlation curves for the ^{11}Be $+d$ inelastic scattering; see black dot-dashed circle area in Fig. 3(b). In principle, using the coincident measurement, we could barely detect the ^{10}Be from breakup reaction at angles smaller than 1.2° due to the energy threshold of the recoil light particles. Therefore, the events in the black dot-dashed circle in Fig. 3(b) should mainly come from the $1n$ stripping reaction of ^{11}Be. As a result, a cut of ^{10}Be laboratory angles larger than 1.2° was applied to extract the breakup cross sections. Other processes, such as evaporation and absorption, can also be eliminated using the coincident measurement, because the low energy deuterons from those reactions would be emitted at the smaller laboratory angles [16].

Figures 4(a) and 4(b) display the excitation energy spectra for the ground state (g.s.) and the continuum states of ^{11}Be, which are deduced from energies and angles of the elastically and inelastically scattered deuterons in coincidence with ^{11}Be and ^{10}Be, respectively. The background contributions arising from ^{12}C and ^{1}H have been subtracted using the data taken from the carbon and $(CH_2)_n$ targets normalized to the same number of beam particles and the equivalent carbon and hydrogen component as for the $(CD_2)_n$ target. The full width at half maximum (FWHM) of the excitation energy spectrum for the elastic scattering is about 2.3 MeV [Fig. 4(a)], resulting from the energy dispersion of the ^{11}Be beam, the energy losses and straggling of the recoil deuterons in the targets, as well as the energy and angular resolution of TELE1. This value agrees with the simulation result using the GEANT4 package [23]. Two regions of excitation energy for the continuum states were selected due to the poor resolution. The first one, ranging from 0.5 to 3.0 MeV, is centered around the known $5/2^+$ resonance at $E_{\text{ex}} = 1.778$ MeV. The second region, from 3.0 to 5.5 MeV, contains other higher energy resonant states, such as the $3/2^+$ state at $E_{\text{ex}} = 3.41$ MeV. The cross sections of the second region could not be extracted from the ^{11}Be $+p$ breakup reaction in Ref. [16] because the solid angle of TELE1 decreases very quickly as the excitation energy increases for that reaction. For the ^{11}Be $+d$ breakup reaction, simulations

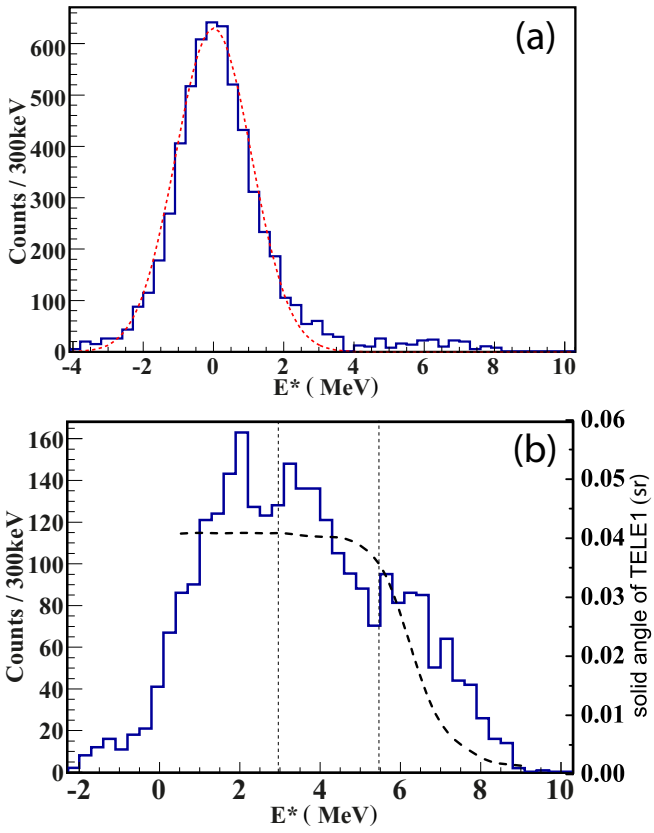

FIG. 4. Excitation energy spectrum for (a) the ground state and (b) unbound excited states of ^{11}Be deduced from the scattered deuterons in coincidence with ^{11}Be and ^{10}Be, respectively. The background contributions arising from ^{12}C and $(CH_2)_n$ have been subtracted. The dashed curve in (b) with the vertical axis on the right-hand side stands for the solid angle of TELE1.

for the solid angle of TELE1 as a function of excitation energy (E_{ex}) were performed with the GEANT4 package, and the results are shown by the dashed line in Fig. 4(b) with the vertical axis on the right-hand side. The solid angle remains nearly a constant from $E_{ex} = 0$–4.5 MeV, and decreases about 10% from $E_{ex} = 4.5$–5.5 MeV. For $E_{ex} > 5.5$ MeV, the solid angle decreases quickly, so the breakup cross sections were not extracted.

The differential cross sections of the ^{11}Be $+d$ elastic scattering, as a ratio to the Rutherford cross sections, are displayed in Fig. 5. The angular distributions of breakup cross sections for the excitation energy intervals of $0.5 < E_{ex} < 3.0$ MeV and $3.0 < E_{ex} < 5.5$ MeV are displayed in Figs. 7(a) and 7(b), respectively. The error bars are purely statistics only taking into consideration the background subtraction of carbon and proton contaminations in the $(CD_2)_n$ target. The systematic error is less than 10%, arising from the uncertainties in solid angles (5%), the thickness of the target (2%), the cuts on the threshold and the particle identification spectrum measured by TELE0 (4%), and the cuts applied on the excitation energy spectra (5%). To monitor the possible deuteron leakage from the $(CD_2)_n$ plastic target, we checked the detected number of recoil deuterons at the beginning and close to the end of

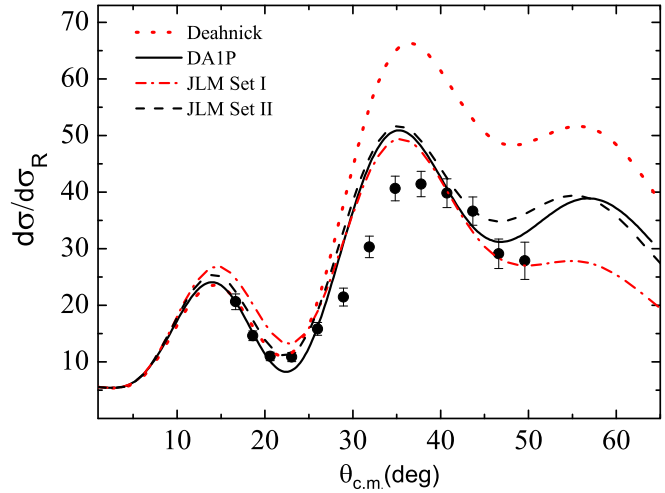

FIG. 5. Comparisons between the experimental differential cross sections (as a ratio to Rutherford) and optical model calculations for the ^{11}Be $+d$ elastic scattering at 26.9A MeV. The dot-dashed, dotted, as well as dashed and solid curves represent the calculations with optical potentials of DA1p, Daehnick *et al.* [24], as well as the folding potential generated with the JLM nucleon-nucleon interaction, with energy-dependence parameters of set I and set II, respectively.

the experiment, respectively, for the same number of incident particles and the same target setup, and found a change of less than 2.0%. This deviation is within the statistical uncertainty. Therefore, the change of C/D ratio in the target is negligible for the present experiment.

III. PHENOMENOLOGICAL OPTICAL MODEL ANALYSIS

In this section, the measured elastic scattering angular distribution is analyzed in the framework of the optical model (OM). There exist in the literature several global deuteron optical model potentials for deuteron scattering, such as that obtained from the comprehensive analysis of Daehnick *et al.* [24]. However, previous analyses have evidenced that these parametrizations fail to properly describe the data when extrapolated outside their initial domain of validity, particularly for light targets and at large scattering angles [25–27]. For this reason, a new global deuteron potential, called DA1p [28], was recently developed, based on 67 sets of experimental data of deuteron elastic scattering from 1p-shell nuclei with incident energies between 5.25 and 170 MeV. This global potential is employed for the present data.

A single-folding model (SFM) analysis was also performed for the elastic scattering data using the Lane-consistent Bruyères Jeukenne-Lejeune-Mahaux (JLM) model nucleon-nucleon interaction. Two sets of energy-dependent parameters, designated as JLM Set I [29] and JLM Set II [30], were applied. The nucleon density distribution of ^{11}Be was calculated with the Hartree-Fock method using the SkX interaction [31]. The calculations from the JLM model, together with those from the systematic optical potentials of DA1p and Daehnick *et al.*, are compared with the experimental angular distributions in Fig. 5.

As shown in Fig. 5, the calculations with the DA1p potential and the folding potential generated with both JLM potentials show reasonable agreement with the experimental differential cross sections. By contrast, the calculation with the Daehnick *et al.* potential overestimates the data. This might indicate that the elastic scattering of deuterons on the weakly bound nuclei could be reproduced by the OM with potentials specially developed for the corresponding incident energy and mass region, or by the SFM including the density of weak-binding nuclei.

IV. XCDCC CALCULATIONS

In this section we compare the measured elastic and breakup cross sections with XCDCC calculations [12,15]. The XCDCC method is a generalization of the standard continuum-discretized coupled-channels (CDCC) formalism which takes into account the effects of core excitation in the structure of the projectile, by including core-excited components in the projectile states, and also in the dynamics of the reaction, by allowing core excitations and deexcitations during the collision. In the present work, this is done by including explicitly the deformation of the ^{10}Be core, within a collective model.

The ^{11}Be structure is described by the particle-rotor model using the Hamiltonian of Ref. [32] (model Be12-b), comprised of central and spin-orbit parts, with the usual Woods-Saxon volume and derivative shapes, respectively. The central part has a fixed geometry ($R_0 = 2.483$ fm, $a = 0.65$ fm) and a parity-dependent strength ($V_c = -54.24$ MeV and -49.67 MeV, for positive and negative parity states, respectively). The spin-orbit part uses the same radius and diffuseness as the central part and a fixed strength $V_{so} = 8.5$ MeV. For the ^{10}Be core, this model assumes a permanent quadrupole deformation $\beta_2 = 0.67$, (i.e., $\delta_2 = \beta_2 R_0 = 1.664$ fm). This model reproduces the separation energies of the two bound states of ^{11}Be as well as the positions of the low-lying narrow $5/2^+$ and $3/2^+$ resonances.

To calculate the energies and wave functions of ^{11}Be we use a pseudostate (PS) method [15], which consists in diagonalizing the Hamiltonian of this composite system in a convenient basis of square-integrable functions. In this work, we use the transformed harmonic oscillator (THO) basis, which is obtained by application of a local scaled transformation (LST) to the traditional harmonic oscillator (HO) basis. The purpose of the LST is to transform the Gaussian asymptotic behavior into an exponential form, which is more convenient for the description of the bound states of the system. In particular, we use the analytical LST proposed in Ref. [33], which was already applied to ^{11}Be in Refs. [15,16,34], and the parameters used in the present calculations are similar to those employed in those references. The size of the basis is determined by the number of oscillator functions (N), the maximum orbital angular momentum for the core-valence motion (ℓ), and the number of core states. In the present calculations we use $N = 12$ and $\ell_{max} = 3$ and the first two states of the core (the g.s. and the first excited state). Continuum states with total angular momentum $J_p^\pi = 1/2^\pm$, $3/2^\pm$, and $5/2^+$ were considered in the calculations. We verified that using a larger value of N or higher values of J_p did not change appreciably the calculated observables. Furthermore, only eigenvalues with energies below 7 MeV were retained in the coupled-channels calculations, since the effect of higher eigenvalues was found to be negligible.

The XCDCC calculations require also the valence-target and core-target interactions. In XCDCC, the core-target interaction (^{10}Be $+d$ in the present case) contains noncentral terms which are responsible for the dynamic core excitation (DCX) mechanism of the core during the collision. To generate this potential, we start from the DA1p parametrization introduced in the previous sections. This potential is deformed with a quadrupole deformation length of $\delta_2 = 1.9$ fm, and expanded in multipoles, retaining the monopole and quadrupole terms. The latter one accounts for the diagonal $2^+ \to 2^+$ and off-diagonal $0^+ \to 2^+$ coupling potentials among the considered ^{10}Be states. To avoid double counting of the ^{10}Be excitation, all parameters are slightly adjusted in order to recover the original description of the ^{10}Be $+d$ elastic scattering data.

In parametrizing the $n + d$ potential one has to deal with the complications arising from the presence of angular-momentum and spin-dependent terms, including tensor forces. Current implementations of the CDCC and XCDCC methods do not allow for these kinds of interaction, so we just derive a simple central $n + d$ potential reproducing some key features of this system. For that, two different prescriptions are used in this work. In our first prescription, the $n + d$ potential is calculated as the folding of $n + p$ and $n + n$ potentials with the ground state of the deuteron. For that, the $n + p$ and $n + n$ interactions were described with the potentials of Manfliet and Tjon [35]. In our second prescription, we parametrize the $n + d$ interaction using the simple Gaussian form

$$U_{nd}(r) = V_G \exp[-(r/a_v)^2] + i W_G \exp[-(r/a_w)^2], \quad (2)$$

with four parameters V_G, W_G, a_v, and a_w adjusted to reproduce the experimental elastic scattering and reaction cross sections for this system at $E_n = 27.5$ MeV [36]. The differences between the ^{11}Be $+d$ observables calculated with these two prescriptions will provide us with an idea of the sensitivity of these observables on the choice of the $n + d$ interaction. The computation of the coupling potentials entering the XCDCC coupled equations and the resolution of these equations were done employing the formalism and codes developed in Ref. [15].

The calculated differential cross sections for the ^{11}Be $+d$ elastic scattering are compared with the experimental data in Fig. 6. The solid and dashed lines are the full XCDCC calculations with the two prescriptions for the $n + d$ interaction, as indicated by the labels. We find a good agreement with the data for c.m. angles up to 30°, and an underestimation beyond this angle. Furthermore, we see that the two prescriptions for the $n + d$ interaction lead to similar results, and their differences cannot explain the observed discrepancy with the data at the largest angles. We also include in this figure the XCDCC calculation omitting the DCX mechanism (dotted line). The sizable difference between this calculation and the full calculation at larger c.m. angles indicates that the DCX has a clear impact on the elastic scattering cross sections for this reaction.

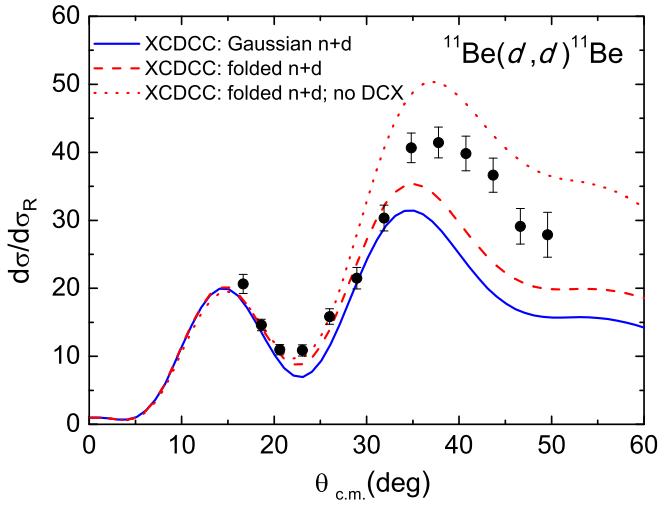

FIG. 6. Experimental and calculated elastic differential cross sections, ratio to Rutherford, for the reaction ^{11}Be $+d$ at 26.9A MeV.

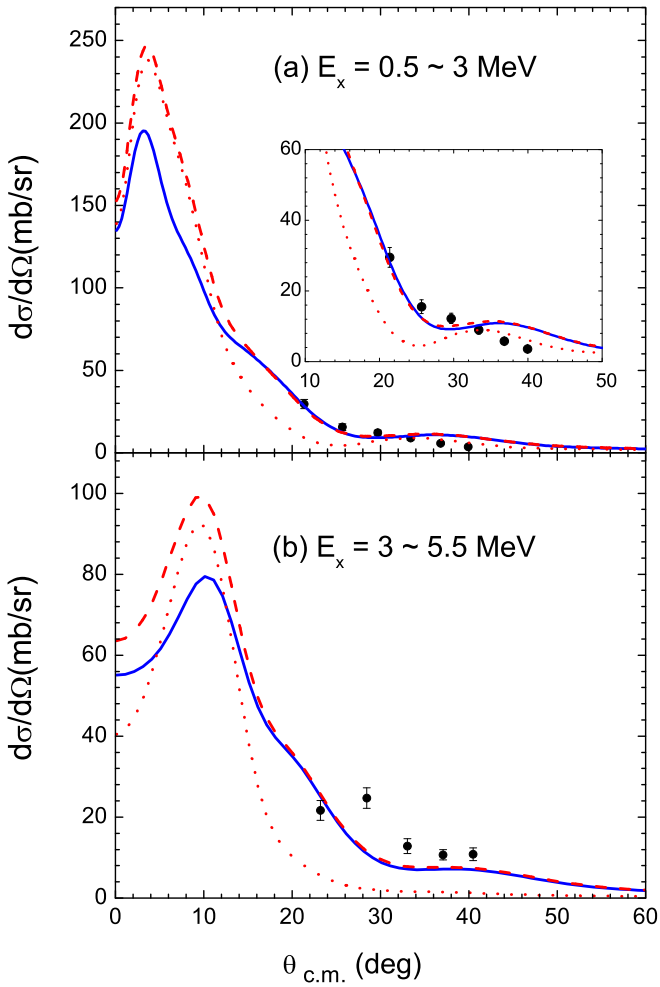

FIG. 7. Experimental and calculated breakup cross sections, as a function of the c.m. scattering angle, for the reaction ^{11}Be $+d$ at 26.9A MeV. The meaning of the lines is the same as in Fig. 6. The inset in (a) amplifies the region containing the experimental data.

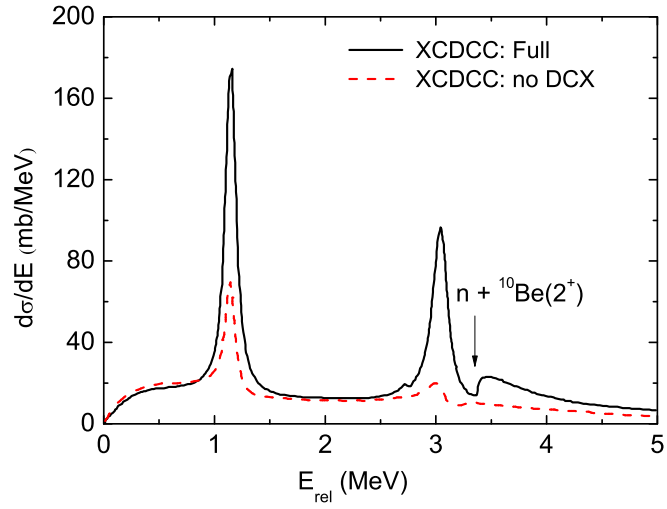

FIG. 8. Energy differential cross section, as a function of the n-^{10}Be relative energy, calculated with the XCDCC method. The solid line is the full XCDCC calculation, whereas the dashed line is the calculation omitting the ^{10}Be $+d$ excitation mechanism. The arrow indicates the excitation energy of the $n + {}^{10}$Be(2$^+$) threshold.

The corresponding breakup angular distributions are compared with the experimental data in Fig. 7. The top and bottom panels correspond to the excitation energy intervals $E_x = 0.5$–3.0 MeV and $E_x = 3.0$–5.5 MeV of ^{11}Be. The meaning of the figures is the same as in Fig. 6. We observe that the two prescriptions for the $n + d$ potential lead to very similar results, particularly at the measured angles. It becomes also apparent that the maximum of the breakup cross section occurs at $\theta_{\text{c.m.}} \approx 10^\circ$, which is outside the range of the measured data. Consequently, the conclusions on the comparison of the calculated and measured breakup data must be taken with the same caution because they are based on a region where the breakup cross section is relatively small and structureless.

Notwithstanding these considerations, one can see that the agreement between the calculations and the data is very reasonable. More interesting is the effect of the DCX mechanism, which can be inferred from the comparison of the full XCDCC calculation with that omitting this effect (dotted line). It is clearly seen that the omission of the DCX gives significantly fewer breakup cross sections. The effect is particulary noticeable for the higher energy interval [Fig. 7(b)], for which the calculation ignoring the DCX mechanism clearly underestimates the data. These effects are qualitatively similar to those found for the $p + {}^{11}$Be reactions at 63.7A MeV [15] and 26.9 MeV [16]. This reinforces the idea that the importance of dynamic core excitations is a general feature of ^{11}Be scattering on light targets.

To get further insight into these results we investigated the breakup cross sections as a function of the relative energy (E_{rel}) of the ^{11}Be system, with respect to the $n + {}^{10}$Be (g.s.) breakup threshold. This is shown in Fig. 8. Note that the XCDCC method provides only a discrete breakup distribution, corresponding to the breakup cross section for each final pseudostate. To obtain a continuous distribution, we convolute

this discrete distribution with the ^{11}Be continuum (scattering) states [37]. The solid line is the result of such a convolution for the full XCDCC calculation. One can see very clearly the two narrow peaks at $E_{\rm rel} \simeq 1.15$ MeV and $E_{\rm rel} \simeq 3$ MeV, which correspond respectively to the low-lying $5/2^+$ and $3/2^+$ resonances. Also noticeable is the sudden increase of the cross section when the excitation energy crosses the threshold $n + {}^{10}\mathrm{Be}(2^+)$. For excitation energies above this threshold, the system can decay either to the ^{10}Be g.s. or to its first excited state (2^+). We include also in this figure the calculation omitting the DCX mechanism (dashed line). The sizable reduction of the cross section is apparent, particularly in the region of the $3/2^+$ resonance, as we observed for the corresponding angular distributions. These results show very clearly the key importance of the DCX mechanism in the $^{11}\mathrm{Be} + d$ reaction.

V. SUMMARY

We measured the elastic scattering and breakup reaction of ^{11}Be on deuterons for the first time at an incident energy of 26.9A MeV. The proton contamination in the $(CD_2)_n$ target was determined by comparing the proton elastic scattering data of ^{11}Be on the $(CD_2)_n$ and $(CH_2)_n$ targets. The measured elastic scattering data were compared with several optical model calculations. We found that the data are well described with a recently developed deuteron potential for 1p-shell nuclei (named DA1p), as well as with single-folding potentials generated with the JLM nucleon-nucleon interaction. On the contrary, the global deuteron potential of Daehnick *et al.* failed to reproduce the data satisfactorily.

An extended version of the XCDCC method, which includes the DCX effects, was also applied to analyze the elastic and breakup data of $^{11}\mathrm{Be} + d$. In the case of the elastic scattering, the full XCDCC calculations including the DCX mechanism reasonably reproduced the experimental cross sections. For the breakup reaction, the full XCDCC calculations significantly increase the calculated cross sections and significantly improve the description of the experimental data with respect to the calculated results omitting DCX effects. The DCX effect is particularly noticeable for the higher excitation energy interval ($E_x = 3$–5.5 MeV), for which the calculation ignoring the DCX mechanism clearly underestimates the data. These results confirm the relevance of the DCX effects in the scattering of weakly bound deformed systems on light targets.

ACKNOWLEDGMENTS

We gratefully acknowledge the staff of the RCNP accelerator group for providing the ^{13}C primary beam and the staff of EN-course for assistance and local support. This work is supported by the 973 Program of China (Grant No. 2013CB834402), the National Natural Science Foundation of China (Grants No. 11275001, No. 11535004, No. 11275011, No. 11275018, and No. U1432247), and China Postdoctoral Science Foundation (Grant No. 20100470133). A.M.M. is partially supported by the Spanish Ministerio de Economía y Competitividad, under Grant No. FIS2014-53448-C2-1-P. J.R. was partially supported by Brazilian Ministerios of Education CAPES and CNPq.

[1] I. Tanihata, H. Savajols, and R. Kanungo, Prog. Part. Nucl. Phys **68**, 215 (2013).
[2] Y. Blumenfeld, T. Nilsson, and P. Van Duppen, Phys. Scr., T **152**, 014023 (2013).
[3] A. Gade, Phys. Scr., T **152**, 014004 (2013).
[4] I. Tanihata, H. Hamagaki, O. Hashimoto, Y. Shida, N. Yoshikawa, K. Sugimoto, O. Yamakawa, T. Kobayashi, and N. Takahashi, Phys. Rev. Lett. **55**, 2676 (1985).
[5] K. T. Schmitt, K. L. Jones, A. Bey, S. H. Ahn, D. W. Bardayan, J. C. Blackmon, S. M. Brown, K. Y. Chae, K. A. Chipps, J. A. Cizewski, K. I. Hahn, J. J. Kolata, R. L. Kozub, J. F. Liang, C. Matei, M. Matoš, D. Matyas, B. Moazen, C. Nesaraja, F. M. Nunes, P. D. O'Malley, S. D. Pain, W. A. Peters, S. T. Pittman, A. Roberts, D. Shapira, J. F. Shriner, M. S. Smith, I. Spassova, D. W. Stracener, A. N. Villano, and G. L. Wilson, Phys. Rev. Lett. **108**, 192701 (2012).
[6] R. Palit, P. Adrich, T. Aumann, K. Boretzky, B. V. Carlson, D. Cortina, U. Datta Pramanik, T. W. Elze, H. Emling, H. Geissel, M. Hellström, K. L. Jones, J. V. Kratz, R. Kulessa, Y. Leifels, A. Leistenschneider, G. Münzenberg, C. Nociforo, P. Reiter, H. Simon, K. Sümmerer, and W. Walus, Phys. Rev. C **68**, 034318 (2003).
[7] I. Talmi and I. Unna, Phys. Rev. Lett. **4**, 469 (1960).
[8] D. E. Alburger, C. Chasman, K. W. Jones, J. W. Olness, and R. A. Ristinen, Phys. Rev. **136**, B916 (1964).
[9] T. Aumann, A. Navin, D. P. Balamuth, D. Bazin, B. Blank, B. A. Brown, J. E. Bush, J. A. Caggiano, B. Davids, T. Glasmacher, V. Guimarães, P. G. Hansen, R. W. Ibbotson, D. Karnes, J. J. Kolata, V. Maddalena, B. Pritychenko, H. Scheit, B. M. Sherrill, and J. A. Tostevin, Phys. Rev. Lett. **84**, 35 (2000).
[10] J. Winfield, S. Fortier, W. Catford, S. Pita, N. Orr, J. V. de Wiele, Y. Blumenfeld, R. Chapman, S. Chappell, N. Clarke, N. Curtis, M. Freer, S. Gals, H. Langevin-Joliot, H. Laurent, I. Lhenry, J. Maison, P. Roussel-Chomaz, M. Shawcross, K. Spohr, T. Suomijrvi, and A. de Vismes, Nucl. Phys. A **683**, 48 (2001).
[11] N. Fukuda, T. Nakamura, N. Aoi, N. Imai, M. Ishihara, T. Kobayashi, H. Iwasaki, T. Kubo, A. Mengoni, M. Notani, H. Otsu, H. Sakurai, S. Shimoura, T. Teranishi, Y. X. Watanabe, and K. Yoneda, Phys. Rev. C **70**, 054606 (2004).
[12] N. C. Summers, F. M. Nunes, and I. J. Thompson, Phys. Rev. C **74**, 014606 (2006).
[13] A. M. Moro and R. Crespo, Phys. Rev. C **85**, 054613 (2012).
[14] R. Crespo, A. Deltuva, and A. M. Moro, Phys. Rev. C **83**, 044622 (2011).
[15] R. de Diego, J. M. Arias, J. A. Lay, and A. M. Moro, Phys. Rev. C **89**, 064609 (2014).
[16] J. Chen, J. L. Lou, Y. L. Ye, Z. H. Li, Y. C. Ge, Q. T. Li, J. Li, W. Jiang, Y. L. Sun, H. L. Zang, N. Aoi, E. Ideguchi, H. J. Ong, Y. Ayyad, K. Hatanaka, D. T. Tran, T. Yamamoto, M. Tanaka,

T. Suzuki, N. T. Tho, J. Rangel, A. M. Moro, D. Y. Pang, J. Lee, J. Wu, H. N. Liu, and C. Wen, Phys. Rev. C **93**, 034623 (2016).

[17] A. Di Pietro, G. Randisi, V. Scuderi, L. Acosta, F. Amorini, M. J. G. Borge, P. Figuera, M. Fisichella, L. M. Fraile, J. Gomez-Camacho, H. Jeppesen, M. Lattuada, I. Martel, M. Milin, A. Musumarra, M. Papa, M. G. Pellegriti, F. Perez-Bernal, R. Raabe, F. Rizzo, D. Santonocito, G. Scalia, O. Tengblad, D. Torresi, A. M. Vidal, D. Voulot, F. Wenander, and M. Zadro, Phys. Rev. Lett. **105**, 022701 (2010).

[18] A. Di Pietro, V. Scuderi, A. M. Moro, L. Acosta, F. Amorini, M. J. G. Borge, P. Figuera, M. Fisichella, L. M. Fraile, J. Gomez-Camacho, H. Jeppesen, M. Lattuada, I. Martel, M. Milin, A. Musumarra, M. Papa, M. G. Pellegriti, F. Perez-Bernal, R. Raabe, G. Randisi, F. Rizzo, G. Scalia, O. Tengblad, D. Torresi, A. M. Vidal, D. Voulot, F. Wenander, and M. Zadro, Phys. Rev. C **85**, 054607 (2012).

[19] A. Shrivastava, Y. Blumenfelda, N. Keeley, T. Zerguerras, T. Aumann, M. Bazin, D. Chromik, G. Crawley, T. Glasmacher, K. Kemper, F. Marchal, D. Morrissey, T. Nakamura, A. Navinb, E. Pollacco, D. Santonocito, B. Sherrill, T. Suomijrvi, M. Thoennessen, E. Tryggestad, and R. Varner, Phys. Lett. B **596**, 54 (2004).

[20] R. Kanungo, A. Gallant, M. Uchida, C. Andreoiu, R. Austin, D. Bandyopadhyay, G. Ball, J. Becker, A. Boston, H. Boston, B. Brown, L. Buchmann, S. Colosimo, R. Clark, D. Cline, D. Cross, H. Dare, B. Davids, T. Drake, M. Djongolov, P. Finlay, N. Galinski, P. Garrett, A. Garnsworthy, K. Green, S. Grist, G. Hackman, L. Harkness, A. Hayes, D. Howell, A. Hurst, H. Jeppesen, K. Leach, A. Macchiavelli, D. Oxley, C. Pearson, B. Pietras, A. Phillips, S. Rigby, C. Ruiz, G. Ruprecht, F. Sarazin, M. Schumaker, A. Shotter, C. Sumitharachchi, C. Svensson, I. Tanihata, S. Triambak, C. Unsworth, S. Williams, P. Walden, J. Wong, and C. Wu, Phys. Lett. B **682**, 391 (2010).

[21] J. G. Johansen, V. Bildstein, M. J. G. Borge, M. Cubero, J. Diriken, J. Elseviers, L. M. Fraile, H. O. U. Fynbo, L. P. Gaffney, R. Gernhäuser, B. Jonson, G. T. Koldste, J. Konki, T. Kröll, R. Krücken, D. Mücher, T. Nilsson, K. Nowak, J. Pakarinen, V. Pesudo, R. Raabe, K. Riisager, M. Seidlitz, O. Tengblad, H. Törnqvist, D. Voulot, N. Warr, F. Wenander, K. Wimmer, and H. De Witte, Phys. Rev. C **88**, 044619 (2013).

[22] T. Shimoda, H. Miyatake, and S. Morinobu, Nucl. Instrum. Methods Phys. Res. Sect. B **70**, 320 (1992).

[23] S. Agostinelli, J. Allison, and K. Amako, Nucl. Instrum. Methods Phys. Res., Sect. A **506**, 250 (2003).

[24] W. W. Daehnick, J. D. Childs, and Z. Vrcelj, Phys. Rev. C **21**, 2253 (1980).

[25] A. C. Betker, C. A. Gagliardi, D. R. Semon, R. E. Tribble, H. M. Xu, and A. F. Zaruba, Phys. Rev. C **48**, 2085 (1993).

[26] C. Bäumer, R. Bassini, A. M. van den Berg, D. De Frenne, D. Frekers, M. Hagemann, V. M. Hannen, M. N. Harakeh, J. Heyse, M. A. de Huu, E. Jacobs, M. Mielke, S. Rakers, R. Schmidt, H. Sohlbach, and H. J. Wörtche, Phys. Rev. C **63**, 037601 (2001).

[27] A. Korff, P. Haefner, C. Bäumer, A. M. van den Berg, N. Blasi, B. Davids, D. De Frenne, R. de Leo, D. Frekers, E.-W. Grewe, M. N. Harakeh, F. Hofmann, M. Hunyadi, E. Jacobs, B. C. Junk, A. Negret, P. von Neumann-Cosel, L. Popescu, S. Rakers, A. Richter, and H. J. Wörtche, Phys. Rev. C **70**, 067601 (2004).

[28] Y. Zhang, D. Y. Pang, and J. L. Lou, Phys. Rev. C **94**, 014619 (2016).

[29] D. Y. Pang, Y. L. Ye, and F. R. Xu, J. Phys. G: Nucl. Part. Phys. **39**, 095101 (2012).

[30] D. Y. Pang, Y. L. Ye, and F. R. Xu, Phys. Rev. C **83**, 064619 (2011).

[31] B. A. Brown, Phys. Rev. C **58**, 220 (1998).

[32] F. M. Nunes, J. A. Christley, I. J. Thompson, R. C. Johnson, and V. D. Efros, Nucl. Phys. A **609**, 43 (1996).

[33] S. Karataglidis, K. Amos, and B. G. Giraud, Phys. Rev. C **71**, 064601 (2005).

[34] J. A. Lay, A. M. Moro, J. M. Arias, and J. Gómez-Camacho, Phys. Rev. C **85**, 054618 (2012).

[35] R. Malfliet and J. Tjon, Nucl. Phys. A **127**, 161 (1969).

[36] P. Schwarz, H. Klages, P. Doll, B. Haesner, J. Wilczynski, B. Zeitnitz, and J. Kecskemeti, Nucl. Phys. A **398**, 1 (1983).

[37] R. de Diego, R. Crespo, and A. M. Moro (unpublished).